Supporting Information

Stuwe et al. 10.1073/pnas.1311081111

SI Text

Helical Repeat Analysis. To investigate the similarities between the N-terminal domain (NTD) of *Chaetomium thermophilum* Nup192 (ctNup192^{NTD}) Armadillo (ARM) repeat module and karyopherin-α (Kap-α) further, we superposed the individual ARM repeats of the ctNup192^{NTD} and compared them with a canonical ARM repeat of Kap-α (Fig. S3*B*). ARM repeats are α-helical sequence motifs consisting of three helices, termed H1, H2, and H3, which are arranged in a triangular pattern that constitutes one turn of a right-handed superhelix (1). All ARM motifs in ctNup192^{NTD} superposed well with the canonical Kap-α ARM repeat, with rmsd values ranging from 1.1 to 4.2 Å. However, the superposition also revealed that the ARM repeats of ctNup192^{NTD} are far more irregular than the ARM repeats of Kap-α. Whereas the ARM repeats of Kap-α are all ∼40 residues in length and can be superposed with very little variation, the ARM repeats of ctNup192^{NTD} occasionally contain long loop decorations or slightly shorter helices, resulting in ARM repeats that range in length from 36 to 83 residues. Based on the structural superposition, we generated a sequence alignment of the ARM repeats and compared it with a recently determined consensus sequence (1). There are 13 positions in canonical ARM repeats where hydrophobic residues are greatly preferred over hydrophilic residues (>90%): one in H1, five in H2, and seven in H3. Although the positions in H1 and H3 are mainly conserved in the ctNup192^{NTD} ARM repeats, H2 is much more divergent, with greater variance in helical length, position, and sequence (Fig. S3*B*). As a result of these deviations, the angles between the helices also vary more than in canonical ARM repeat proteins.

Similarly, the Huntingtin, EF3, PP2A, and TOR1 (HEAT) module could generally be superposed with other HEAT repeat-containing proteins, such as CRM1, and a structure-based sequence alignment reveals that the consensus hydrophobic positions in helices αA and αB are conserved, as identified previously (1). There are nine positions in canonical HEAT repeats where hydrophobic residues are greatly preferred, and we found that these positions were largely conserved in the HEAT repeats of ctNup192^{NTD} (Fig. S3*C*). Whereas HEAT repeats 2 and 3 have relatively normal helical lengths, HEAT repeat 1 is unusual in that its helices are 34 and 28 residues long, compared with the 13 and 17 residues observed in canonical HEAT repeats. This feature is evolutionarily conserved in fungal Nup192 proteins (Fig. S2). The N-terminal half of helix α9 and the C-terminal half of helix α10 participate in the HEAT superhelix, whereas the rest of the helices protrude from the structure (Fig. 1*B*).

Conformational Plasticity. Many extended α-helical solenoids, including members of the β-karyopherin family, exhibit extensive conformational flexibility (2–5). When we performed a structural superposition of the two ctNup192^{NTD} molecules in the asymmetrical unit, we observed two different conformations (Fig. S4). The two molecules can be superposed with an rmsd of 1.2 Å over 778 Cα atoms, but the N-terminal and C-terminal halves can be superposed separately with rmsd values of 0.3 Å over 259 Cα atoms and 0.6 Å over 403 Cα atoms, respectively. The gap between the N-terminal HEAT module and the C-terminal ARM module in the two ctNup192^{NTD} structures differs by ∼4 Å as a result of a rigid body rotation of the N-terminal Head and HEAT modules away from the C-terminal ARM module (Fig. S4*A*). This conformational change is mediated by the hinge module, which includes helices α15 and α16, and the long hinge loop that follows these helices and caps the HEAT and ARM modules (Fig. S4*C*).

Further conformational changes were apparent when the structures of ctNup192^{NTD} were compared with the recently determined structure of *Saccharomyces cerevisiae* Nup192^{NTD} (scNup192^{NTD}) (6). scNup192^{NTD} possesses a similar overall architecture and can be superposed onto ctNup192^{NTD} with an rmsd of 3.5 Å over 646 Cα atoms. However, the N-terminal half of the molecule is rotated away from the C-terminal half, resulting in a gap between the two halves that opens an additional ∼5 Å to a total distance of ∼18 Å (Fig. S4*A*). This is most apparent when the N- and C-terminal halves of the ring are superposed separately, which results in substantially lower rmsd values of 2.9 Å over 232 Cα atoms and 2.3 Å over 375 Cα atoms, respectively. Moreover, the hinge axis is not parallel to the equatorial plane of the Nup192^{NTD} ring, and it facilitates not only an increase of the ring gap but a rotation of the Head and HEAT modules by ∼26° out of the equatorial plane of the ring (Fig. S4*A*). As such, the observed conformational changes are more similar to the opening of a lock washer than to the opening of a clamp. Again, the hinge module mediates these conformational changes, but, surprisingly, the scNup192^{NTD} hinge loop adopts a substantially different conformation and no longer contacts the C-terminal three ARM repeats (Fig. S4*D*).

The conformational changes of the hinge loop are very similar to the observed relocation of the acidic loop in the export β-karyopherin CRM1 (4, 5, 7). Like the hinge loop of ctNup192^{NTD}, the acidic loop of CRM1 displays species-dependent variation in sequence and length. Furthermore, the CRM1 acidic loop occupies a similar position within the CRM1 ring as the hinge loop does in the ctNup192^{NTD} ring and also makes extensive contacts within the concave surface (4, 5, 7). Although the conformational changes observed here for ctNup192^{NTD} are not as dramatic, it is nevertheless conceivable that they play an important role in regulating the interactions with other adaptor nucleoporins.

Together, these observations provide further evidence for an evolutionary relationship between Nup192 and the flexible β-karyopherins.

SI Methods

Protein Expression and Purification. DNA fragments encoding ctNup192^{NTD} (residues 1–958), ctNup192 C-terminal domain Nup192^{CTD} (residues 976–1,756), Nup192$^{\Delta HEAD}$ (residues 153–958), and Nup192^{TAIL} (residues 1,416–1,756) were amplified by PCR and cloned into a modified pET28a vector, which contains an N-terminal hexahistidine tag followed by a PreScission protease cleavage site, using NdeI and NotI restriction sites (8). DNA fragments encoding residues 1–90 and 31–67 of ctNup53 and residues 262–301 of ctNic96 were cloned into modified pET28a or multi-cloning and expression (pET-MCN) vectors containing an N-terminal hexahistidine-SUMO (small ubiquitin-like modifier) tag, using BamHI and NotI restriction sites (9, 10). A DNA fragment encoding *C. thermophilum* Nup188^{NTD} (residues 1–1,134) was cloned into the modified pET28a vector with an N-terminal hexahistidine-SUMO tag, using AseI and BamHI restriction sites. The *S. cerevisiae* Kap-α expression construct was a kind gift from Elena Conti (Max Planck Institute of Biochemistry, Martinsried, Germany) (11). The details of the bacterial expression constructs are listed in Tables S2 and S3.

All proteins were expressed in *Escherichia coli* BL21-CodonPlus (DE3)-RIL cells (Stratagene) in Terrific Broth media. Seleno–L-methionine–labeled protein was produced in a synthetic medium that suppresses methionine biosynthesis, following standard protocols (12). ctNup192 and ctNup188 fragment expression was induced at an OD_{600} of 0.6 with 0.5 mM isopropyl-β-D-thiogalactopyranoside (IPTG) at 37 °C for 3 h. Expression of ctNup53 and ctNic96 fragments was induced at an OD_{600} of 0.8 with 0.5 mM IPTG at 18 °C for 16 h. Cells were harvested by centrifugation and resuspended in a buffer containing 20 mM Tris (pH 8.0), 500 mM NaCl, 15 mM imidazole, 4 mM β-mercaptoethanol (β-ME), and complete EDTA-free protease inhibitor mixture (Roche).

For purification of all proteins, the cells were lysed with a cell disruptor (Avestin) and DNase I (Roche) was added to the lysate before centrifugation at 30,000 × g for 1 h. The supernatant was filtered through a 0.45-μm filter (Millipore) and loaded onto a nickel-nitrilotriacetic acid (Ni-NTA) column (GE Healthcare) equilibrated in buffer A [20 mM Tris (pH 8.0), 500 mM NaCl, 15 mM imidazole, and 4 mM β-ME]. Protein was eluted with a linear gradient of buffer B [20 mM Tris (pH 8.0), 500 mM NaCl, 500 mM imidazole, and 4 mM β-ME]. Protein-containing fractions were pooled and incubated overnight with PreScission or ULP1 protease at 4 °C while dialyzing against buffer A. Digested protein was loaded onto a Mono Q 10/100 GL ion-exchange column (GE Healthcare) equilibrated in a buffer containing 20 mM Tris (pH 8.0), 100 mM NaCl, and 5 mM DTT. Protein was eluted using a linear gradient of a buffer containing 20 mM Tris (pH 8.0), 2.0 M NaCl, and 5 mM DTT; concentrated in a centrifugal filter (Millipore); and loaded on a HiLoad Superdex 200 16/60 gel filtration column (GE Healthcare) equilibrated in a buffer containing 20 mM Tris (pH 8.0), 100 mM NaCl, and 5 mM DTT. Protein-containing fractions were pooled and concentrated to 20 mg/mL for crystallization or biochemical studies.

Fractions from Ni-NTA elution containing ctNup53 or ctNic96 SUMO-fusion proteins were dialyzed against a buffer containing 20 mM Tris (pH 8.0), 100 mM NaCl, and 5 mM DTT and were loaded onto a Mono Q 10/100 GL column; eluted with a linear gradient of a buffer containing 20 mM Tris (pH 8.0), 2.0 M NaCl, and 5 mM DTT; concentrated in a centrifugal filter (Millipore); and loaded onto a Superdex 200 10/300 GL gel filtration column (GE Healthcare). Protein containing-fractions were pooled and concentrated for biochemical studies.

ctNup53 and ctNup192 mutants were generated by QuikChange mutagenesis, confirmed by DNA sequencing, and expressed and purified as the WT proteins. The $ctNup192^{TAIL}$•$ctNic96^{H2}$ complex was generated by coexpression of the two proteins and purified with the same protocol as $ctNup192^{TAIL}$. *S. cerevisiae* Kap-α was expressed and purified as previously described (11).

Protein Crystallization and Data Collection. Protein crystallization was carried out at 21 °C in hanging drops consisting of 1.0 μL of protein solution and 1.0 μL of reservoir solution. Crystals appeared in the tetragonal space group $P4_32_12$, with two molecules in the asymmetrical unit. These crystals were improved by microseeding, which produced crystals that grew to maximum dimensions of ∼100 × 100 × 300 μm^3 in 1 wk. Crystals used for diffraction experiments were grown in 0.1 M MES (pH 5.7), 0.6 M $MgCl_2$, and 5% (wt/vol) PEG 4000, with a protein concentration of 20 mg/mL seleno–L-methionine–labeled crystals grown under identical conditions. Native crystals we derivatized in the crystallization drop by adding 0.1 μL of a saturated $[Ta_6Br_{12}]^{2+}$ cluster solution, followed by 16 h of incubation before freezing. Crystals were cryoprotected by gradually supplementing the drop in 2% steps to 24% (vol/vol) ethylene glycol and flash-frozen in liquid nitrogen. X-ray diffraction data were collected at 100 K at beam line 12-2 at the Stanford Synchrotron Radiation Lightsource.

Structure Determination and Refinement. X-ray diffraction data were processed with the HKL2000 denzo/scalepack package and XDS (13, 14). Initial phases were calculated in PHASER using single anomalous dispersion X-ray diffraction data obtained from a Ta_6Br_{12} cluster derivative. These phases were used to locate 59 selenium atoms in anomalous X-ray diffraction data obtained from a seleno–L-methionine–labeled crystal (15). Solvent flattening and noncrystallographic symmetry (NCS) averaging were performed in Resolve to improve phases of the seleno–L-methionine–labeled derivative (16, 17). The experimental map was of excellent quality and allowed for unambiguous placement of all helices and sequence assignment, aided by the positions of the selenium atoms (Fig. S1). Iterative rounds of model building and refinement were performed with Phenix (16) and Coot (18). Initial rounds of refinement were performed with NCS restraints and individual isotropic B-factor refinement. Final refinement rounds were performed without NCS restraints, with hydrogen atoms as riding atoms and with translation/libration/screw (TLS) groups identified by TLSMD (19). The final model was refined to 2.7-Å resolution with R_{work} and R_{free} values of 19.1% and 23.1%, respectively. No density was observed for residues 174–180, 569–589, and 680–698 and for residues 64–66, 170–181, 537–547, 567–587, 678–698, 804–820, and 894–916 for the first and second molecules in the asymmetrical unit, respectively. These residues are presumed to be disordered and have been omitted from the final model. The stereochemical quality was assessed with PROCHECK and MolProbity, and there were no Ramachandran outliers detected by either program (20, 21). Details of the data collection and refinement statistics are provided in Table S1.

Multiangle Light Scattering. Purified $ctNup192^{NTD}$ was characterized by multiangle light scattering following size-exclusion chromatography (SEC) (22). $ctNup192^{NTD}$ (750 μg) was injected onto a Superdex 200 10/300 GL gel filtration chromatography column equilibrated in a buffer containing 20 mM Tris (pH 8.0), 100 mM NaCl, and 5 mM DTT. The chromatography system was connected in series with an 18-angle light-scattering detector (DAWN HELEOS II; Wyatt Technology), a dynamic light-scattering detector (DynaPro Nanostar; Wyatt Technology), and a refractive index detector (Optilab t-rEX; Wyatt Technology). Data were collected every 1 s at a flow rate of 0.5 mL/min at 25 °C. Data analysis was carried out using the program ASTRA 6, yielding the molar mass and mass distribution (polydispersity) of the sample.

Analytical SEC. Protein interaction experiments were carried out on a Superdex 200 10/300 GL gel filtration column equilibrated in a buffer containing 20 mM Tris (pH 8.0), 100 mM NaCl, and 5 mM DTT. Threefold molar excess of N-terminal SUMO-fused $ctNic96^{H2}$ or $ctNup53^{N}$ was mixed with $ctNup192^{NTD}$ or $ctNup192^{CTD}$ and incubated for 30 min on ice. In the case of the interaction analysis for $ctNup53^{N}$ with Kap-α, a fourfold molar excess of the N-terminal SUMO-fused $ctNup53^{N}$ was mixed with Kap-α and incubated for 30 min on ice. Complex formation was monitored by injection of the preincubated proteins or the individual components onto the gel filtration column. The $ctNup53^{31–67}$ competition experiment was performed by preincubating $ctNup192^{NTD}$ with a purified, stoichiometric complex of Kap-α•$ctNup53^{N}$. Interaction tests using $ctNup53^{31–67}$ and $ctNup192^{NTD}$ variants were performed similarly. To assay the interaction between $ctNup192^{TAIL}$ and $ctNic96^{H2}$, equal amounts of $ctNup192^{TAIL}$ or the purified $ctNup192^{TAIL}$•$ctNic96^{H2}$ heterodimer were injected onto the gel filtration column. All proteins were analyzed under identical buffer conditions, and complex formation was confirmed by SDS/PAGE of the protein-containing fractions, followed by Coomassie brilliant blue staining.

Isothermal Titration Calorimetry. Isothermal titration calorimetry (ITC) measurements were performed at 21 °C using a VP-ITC calorimeter (GE Healthcare) and consisted of 30 injections of

10 μL with a spacing of 180 s. Reference power was 10 μcal/s for titrations with ctNup192^{NTD} and 20 μcal/s for titrations with Kap-α. For titrations with ctNup192^{NTD} variants, 200 μM ctNup53$^{31–67}$ was injected into 10 μM ctNup192^{NTD}. For titrations with Kap-α, 1.5 mM ctNup53$^{31–67}$ was injected into 150 μM Kap-α. Titrations using WT proteins were performed in triplicate. Heat from dilution was subtracted for baseline correction. All data were analyzed using Origin 7.0 software with MicroCal add-ons.

Yeast Strains. The ORF of Nup192 in the *S. cerevisiae* haploid strain BY4741 was replaced with the HIS3 cassette by homologous recombination as previously described (23). Due to the lethality of the *NUP192* KO, the BY4741 strain was complemented with a pRS416 construct carrying full-length *S. cerevisiae NUP192* with an N-terminal mCherry tag under the control of the *NOP1* promoter. Subsequently, pRS415-GFP constructs carrying various Nup192 variants were introduced. The transformants were selected twice on synthetic dextrose complete (SDC)-leucine (Leu) plates containing 5-fluoroorotic acid (5-FOA; Bio Gold) to ensure the loss of the pRS416-mCherry-*NUP192* construct before analysis. The details of the yeast expression constructs are listed in Tables S2 and S3.

The strain carrying the Nup53 plasmids in a double-deletion background was generated as follows. The *NUP53* deletion was introduced into BY4741 *nup59*::kanMX4 (Open Biosystems) and covered with pRS416-mCherry-*NUP53*, resulting in the strain *nup53*Δ*nup59*Δ (*MAT*α *his3*Δ*1 leu2*Δ*0 ura3*Δ*0 nup59*::kanMX4 *nup53*::HIS3 pRS416-mCherry-*NUP53*). This strain was transformed with the plasmid pRS415-GFP-*NUP53* or pRS415-GFP-*nup53*^{F124A}, and transformants were selected twice on SDC-Leu plates containing 5-FOA.

Yeast Analyses. For viability analysis, *S. cerevisiae* strains carrying GFP-Nup192 variants were grown at 30 °C to midlog phase in SDC-Leu media and diluted to 10 million cells per milliliter. This stock was used to generate a 10-fold dilution series, of which 5 μL was spotted on SDC-Leu and 5-FOA/SDC-Leu plates and grown at 30 °C for 2–4 d, respectively. For growth analysis of the shuffled strains, the same dilutions were prepared; spotted on yeast extract peptone dextrose (YPD) plates; and grown at 21 °C, 30 °C, and 37 °C for 2–4 d. For localization analysis, live cells were analyzed using a Carl Zeiss Observer Z.1 equipped with a Hamamatsu camera C10600 Orca-R^2.

FISH mRNA Export Assay. Liquid cultures of single-deletion yeast strains carrying GFP-fusion proteins of Nup192 were grown overnight at 30 °C in SDC-Leu media to an OD_{600} of 0.4 and subsequently shifted to 37 °C for 4 h before fixation in formaldehyde. These cells were then analyzed by FISH using an Alexa-647–labeled 50-mer oligo dT probe as previously described (24, 25). The statistical analysis was carried out using six independent images with at least 100 cells each.

EM Docking. The structure of ctNup192^{NTD} was manually placed into the EM envelope of full-length ctNup192, taking advantage of the published localization of the N terminus, as determined by dynein light chain-interacting domain-dynein light chain 2 (DID-Dyn2) labeling (26). This initial placement was then refined against the EM envelope using the rigid body refinement routine in MolRep (27).

Illustration and Figures. Sequence alignments were generated using ClustalX and colored with ALSCRIPT (28, 29). Structural figures were generated using PyMOL (www.pymol.org), and the electrostatic potential was calculated with the Adaptive Poisson–Boltzmann Solver (30).

1. Kippert F, Gerloff DL (2009) Highly sensitive detection of individual HEAT and ARM repeats with HHpred and COACH. *PLoS ONE* 4(9):e7148.
2. Chook YM, Blobel G (1999) Structure of the nuclear transport complex karyopherin-beta2-Ran x GppNHp. *Nature* 399(6733):230–237.
3. Cingolani G, Petosa C, Weis K, Müller CW (1999) Structure of importin-beta bound to the IBB domain of importin-alpha. *Nature* 399(6733):221–229.
4. Monecke T, et al. (2009) Crystal structure of the nuclear export receptor CRM1 in complex with Snurportin1 and RanGTP. *Science* 324(5930):1087–1091.
5. Monecke T, et al. (2013) Structural basis for cooperativity of CRM1 export complex formation. *Proc Natl Acad Sci USA* 110(3):960–965.
6. Sampathkumar P, et al. (2013) Structure, dynamics, evolution, and function of a major scaffold component in the nuclear pore complex. *Structure* 21(4):560–571.
7. Dong X, et al. (2009) Structural basis for leucine-rich nuclear export signal recognition by CRM1. *Nature* 458(7242):1136–1141.
8. Hoelz A, Nairn AC, Kuriyan J (2003) Crystal structure of a tetradecameric assembly of the association domain of Ca2+/calmodulin-dependent kinase II. *Mol Cell* 11(5):1241–1251.
9. Mossessova E, Lima CD (2000) Ulp1-SUMO crystal structure and genetic analysis reveal conserved interactions and a regulatory element essential for cell growth in yeast. *Mol Cell* 5(5):865–876.
10. Romier C, et al. (2006) Co-expression of protein complexes in prokaryotic and eukaryotic hosts: Experimental procedures, database tracking and case studies. *Acta Crystallogr D Biol Crystallogr* 62(Pt 10):1232–1242.
11. Conti E, Uy M, Leighton L, Blobel G, Kuriyan J (1998) Crystallographic analysis of the recognition of a nuclear localization signal by the nuclear import factor karyopherin alpha. *Cell* 94(2):193–204.
12. Doublié S (2007) Production of selenomethionyl proteins in prokaryotic and eukaryotic expression systems. *Methods Mol Biol* 363:91–108.
13. Kabsch W (2010) XDS. *Acta Crystallogr D Biol Crystallogr* 66(Pt 2):125–132.
14. Otwinowski Z, Minor W (1997) Processing of X-ray diffraction data collected in oscillation mode. *Methods Enzymol* 276:307–326.
15. McCoy AJ, et al. (2007) Phaser crystallographic software. *J Appl Cryst* 40(Pt 4):658–674.
16. Adams PD, et al. (2010) PHENIX: A comprehensive Python-based system for macromolecular structure solution. *Acta Crystallogr D Biol Crystallogr* 66(Pt 2):213–221.
17. Terwilliger TC (2000) Maximum-likelihood density modification. *Acta Crystallogr D Biol Crystallogr* 56(Pt 8):965–972.
18. Emsley P, Cowtan K (2004) Coot: Model-building tools for molecular graphics. *Acta Crystallogr D Biol Crystallogr* 60(Pt 12 Pt 1):2126–2132.
19. Painter J, Merritt EA (2006) Optimal description of a protein structure in terms of multiple groups undergoing TLS motion. *Acta Crystallogr D Biol Crystallogr* 62(Pt 4):439–450.
20. Laskowski RA, Macarthur MW, Moss DS, Thornton JM (1993) Procheck—A program to check the stereochemical quality of protein structures. *J Appl Crystallogr* 26(Pt 2):283–291.
21. Davis IW, et al. (2007) MolProbity: All-atom contacts and structure validation for proteins and nucleic acids. *Nucleic Acids Res* 35(Web Server issue):W375–W383.
22. Wyatt PJ (1997) Multiangle light scattering: The basic tool for macromolecular characterization. *Instrum Sci Technol* 25(1):1–18.
23. Sikorski RS, Hieter P (1989) A system of shuttle vectors and yeast host strains designed for efficient manipulation of DNA in Saccharomyces cerevisiae. *Genetics* 122(1):19–27.
24. Gwizdek C, et al. (2006) Ubiquitin-associated domain of Mex67 synchronizes recruitment of the mRNA export machinery with transcription. *Proc Natl Acad Sci USA* 103(44):16376–16381.
25. Seo HS, et al. (2009) Structural and functional analysis of Nup120 suggests ring formation of the Nup84 complex. *Proc Natl Acad Sci USA* 106(34):14281–14286.
26. Amlacher S, et al. (2011) Insight into structure and assembly of the nuclear pore complex by utilizing the genome of a eukaryotic thermophile. *Cell* 146(2):277–289.
27. Vagin A, Teplyakov A (2010) Molecular replacement with MOLREP. *Acta Crystallogr D Biol Crystallogr* 66(Pt 1):22–25.
28. Jeanmougin F, Thompson JD, Gouy M, Higgins DG, Gibson TJ (1998) Multiple sequence alignment with Clustal X. *Trends Biochem Sci* 23(10):403–405.
29. Barton GJ (1993) ALSCRIPT: A tool to format multiple sequence alignments. *Protein Eng* 6(1):37–40.
30. Baker NA, Sept D, Joseph S, Holst MJ, McCammon JA (2001) Electrostatics of nanosystems: Application to microtubules and the ribosome. *Proc Natl Acad Sci USA* 98(18):10037–10041.

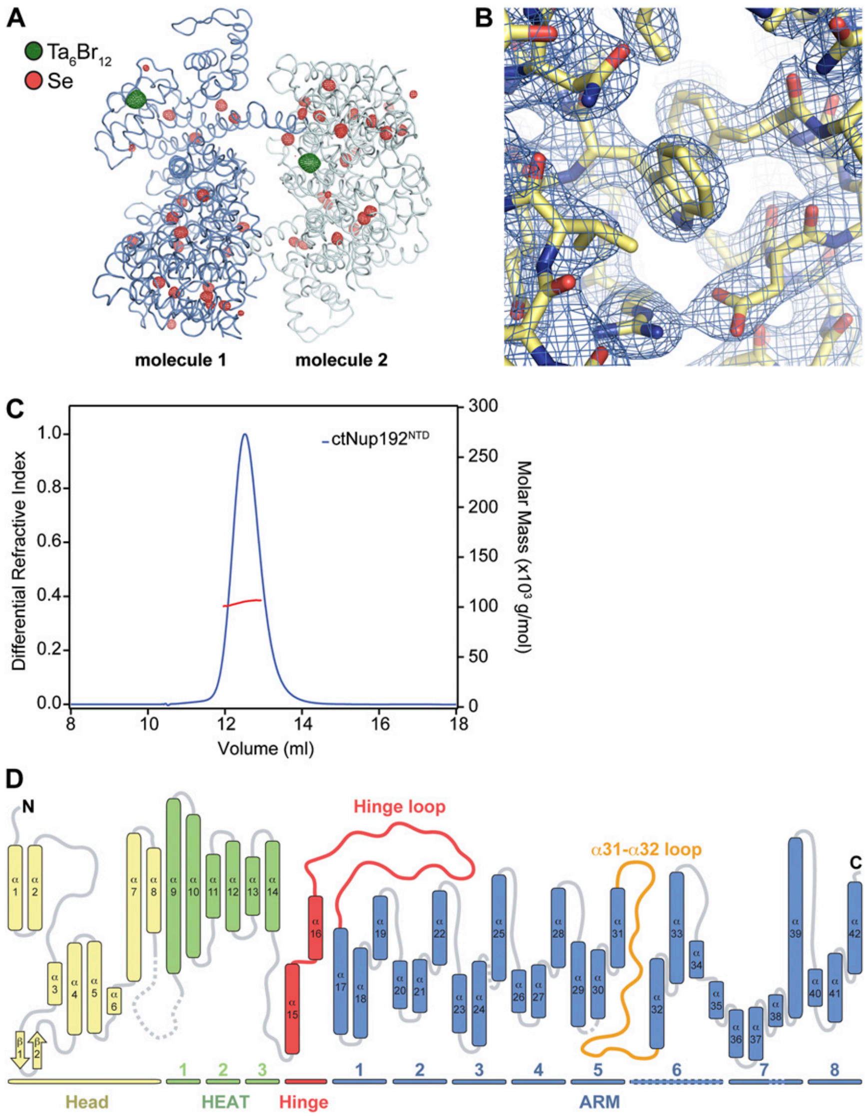

Fig. S1. Structure determination and oligomeric state analysis of ctNup192[NTD]. (*A*) Two molecules in the asymmetrical unit are shown in a ribbon representation and colored in blue and light blue. Anomalous difference Fourier maps of the Ta_6Br_{12} cluster (green) and seleno–L-methionine–labeled protein (red) derivatives are contoured at 10.0 σ and 5.0 σ, respectively. (*B*) Representative final $2|F_O| - |F_C|$ density map contoured at 1.0 σ. (*C*) Size exclusion chromatography coupled multiangle light scattering (SEC-MALS) analysis of ctNup192[NTD]. The normalized differential refractive index (blue) is plotted against the elution volumes from a Superdex 200 10/300 GL gel filtration column and overlaid with the experimental molecular mass for the peak fractions (red). The determined molecular mass for ctNup192[NTD] is 105.0 kDa (the theoretical molecular mass is 108.8 kDa). (*D*) Schematic representation of the α-helical motifs identified in ctNup192[NTD]. The Head module includes helices α1–α8 and a β-hairpin composed of β-strands β1–β2. The HEAT module is composed of three HEAT repeats, helices α9–α14, and is connected to the ARM module via the hinge module, which contains helices α15 and α16. The ARM module contains eight turns of a right-handed superhelix composed of helices α17–α42. HEAT and ARM repeats are numbered and highlighted below the helices, with dashed lines indicating deviations from canonical ARM repeats.

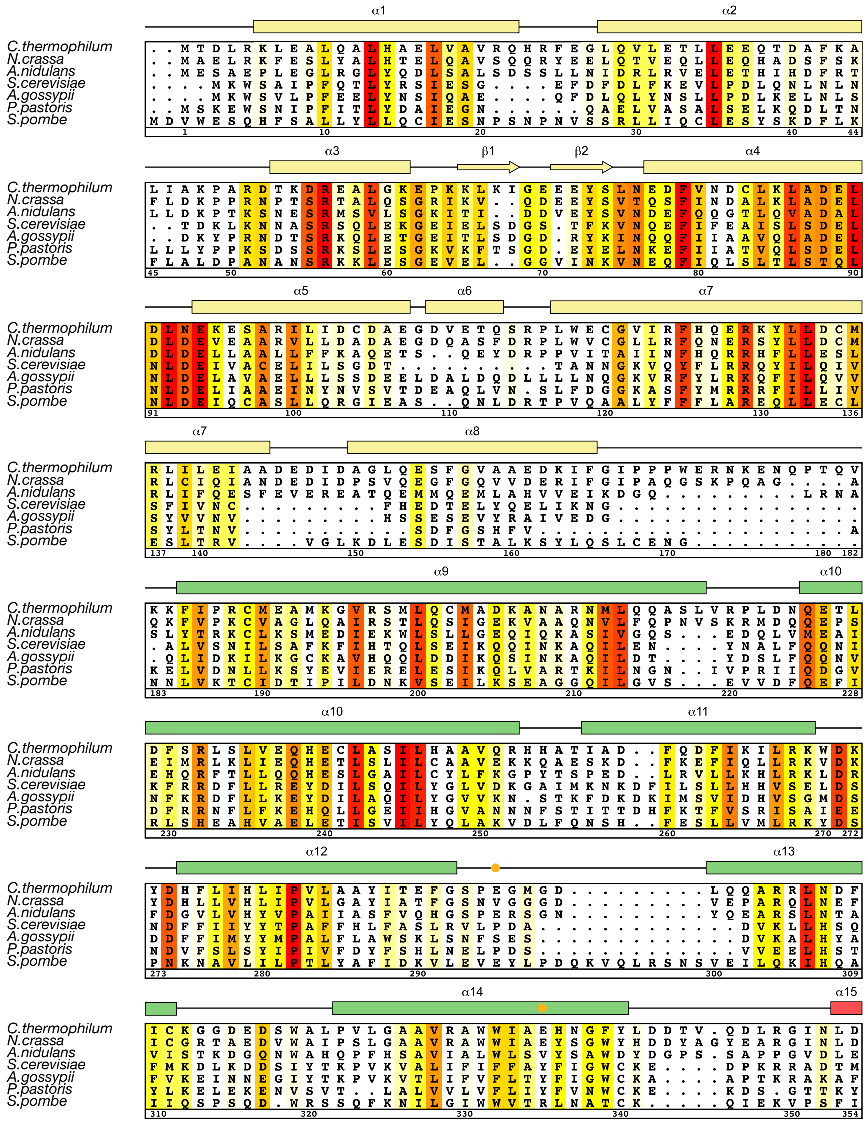

Fig. S2. (Continued)

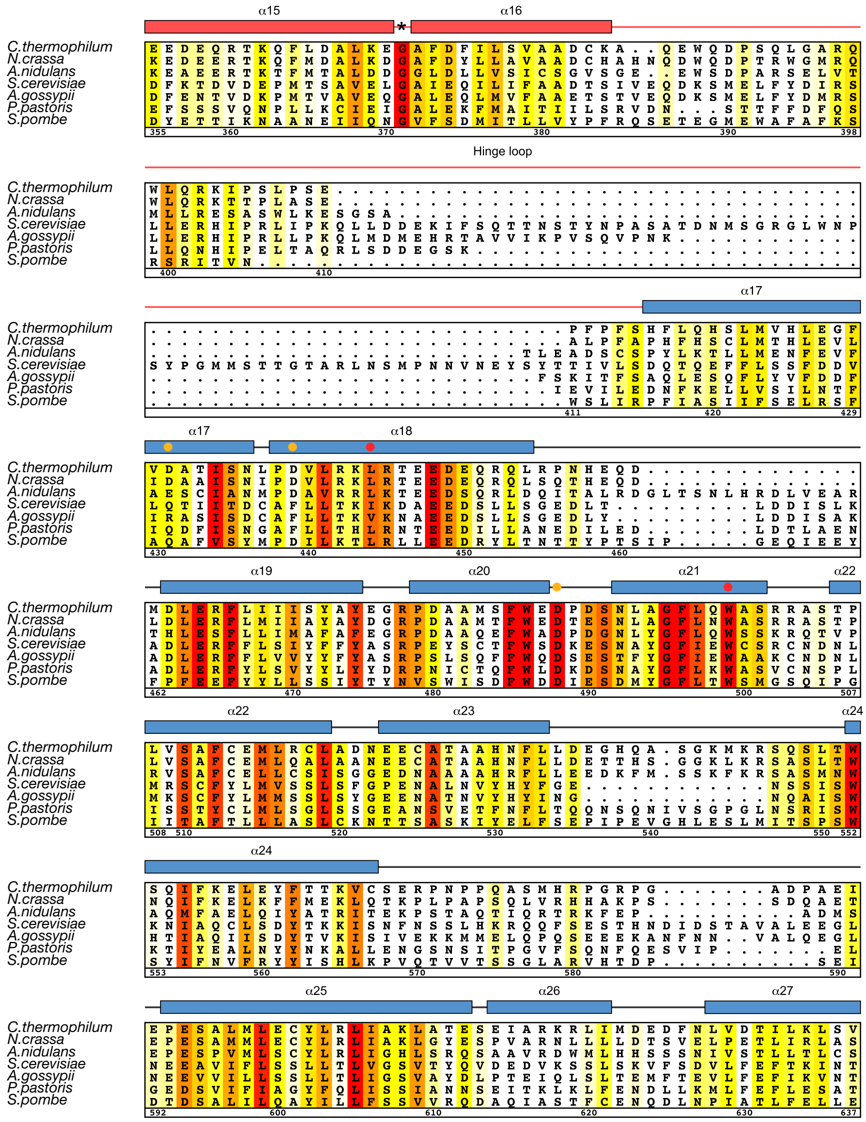

Fig. S2. (Continued)

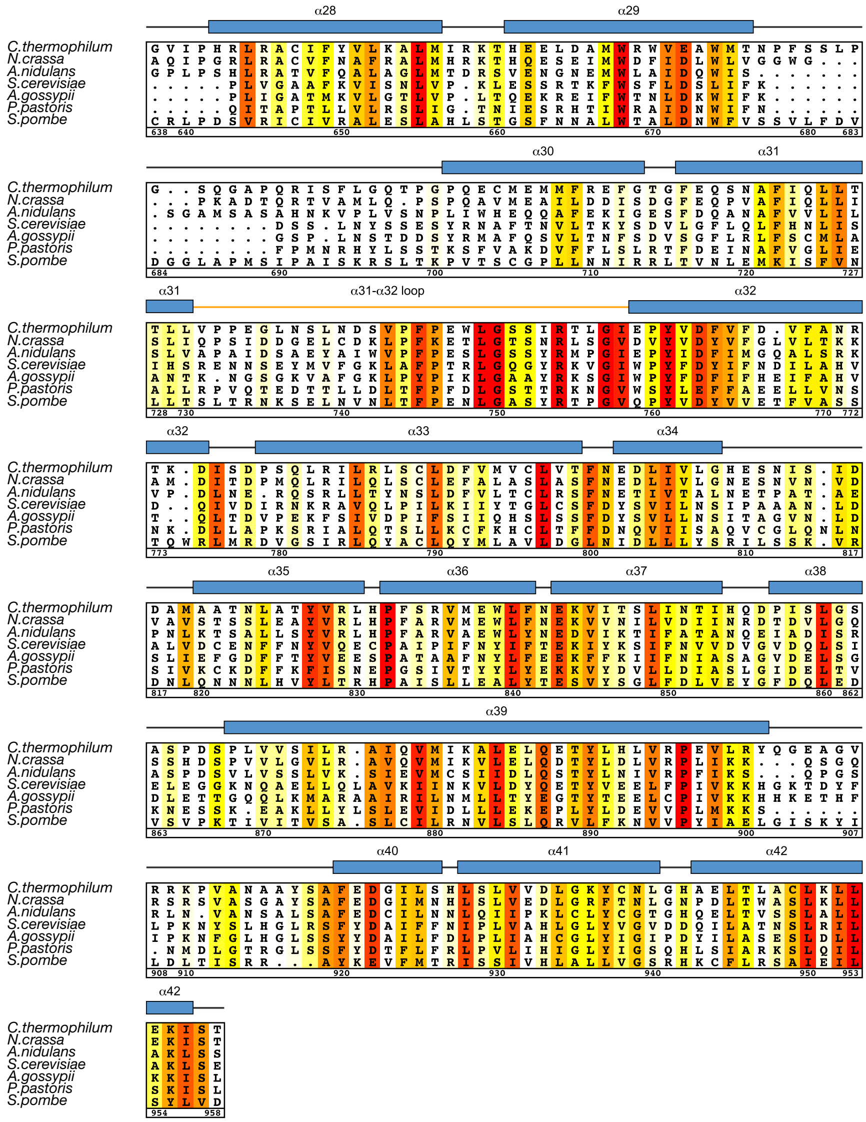

Fig. S2. Multispecies sequence alignment of Nup192^{NTD}. Seven diverse fungal species were aligned and colored by sequence similarity according to the BLOSUM62 (Blocks Substitution Matrix) matrix from white (less than 45% similarity), to yellow (45% similarity), to red (100% identity). The numbering is according to ctNup192^{NTD}. The secondary structure is indicated above the sequence as rectangles (α-helices), arrows (β-strands), and lines (unstructured regions). Secondary structure elements are colored according to the scheme used in Fig. 1. Dots in the secondary structure plot indicate residues that reduce (orange) or completely disrupt (red) the ctNup53 interaction upon mutation to alanine. An asterisk indicates the position of the invariant glycine 371 between hinge helices α15 and α16.

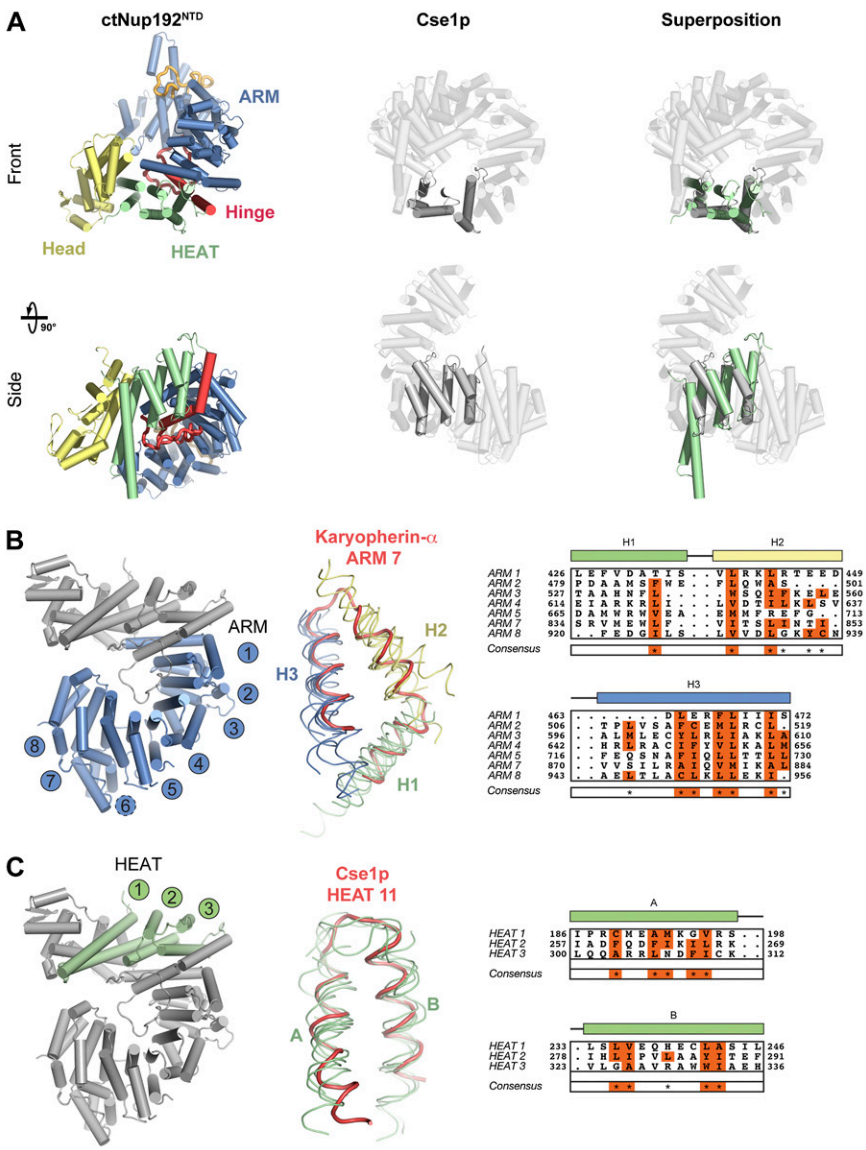

Fig. S3. Analyses of the ARM and HEAT repeats in ctNup192^{NTD}. (*A*, *Upper*) Overview of the structures of ctNup192^{NTD} (*Left*) and Cse1p [*Center*, gray; Protein Data Bank (PDB) ID code 1WA5] (1), and their superposition (*Right*). (*A*, *Lower*) Depiction of 90° rotated views of the above structures. (*B*, *Left*) Overview of the ctNup192^{NTD} structure is shown, with the ARM repeats highlighted in blue. The structural superposition of the ctNup192^{NTD} ARM repeats and ARM repeat 7 of Kap-α (PDB ID code 1BK5) (2) (*Center*) and the structure-guided sequence alignment (*Right*) are shown. Consensus hydrophobic positions are indicated below with asterisks, and those residues that match these positions are highlighted in red. (*C*) ctNup192^{NTD} HEAT repeats are highlighted in green (*Left*), and their structural superposition with HEAT repeat 11 from Cse1p (PDB ID code 1WA5) (1) is shown (*Center*). (*Right*) Structure-guided sequence alignment is shown, with consensus hydrophobic positions highlighted as in *B*.

1. Matsuura Y, Stewart M (2004) Structural basis for the assembly of a nuclear export complex. *Nature* 432(7019):872–877.
2. Conti E, Uy M, Leighton L, Blobel G, Kuriyan J (1998) Crystallographic analysis of the recognition of a nuclear localization signal by the nuclear import factor karyopherin alpha. *Cell* 94(2):193–204.

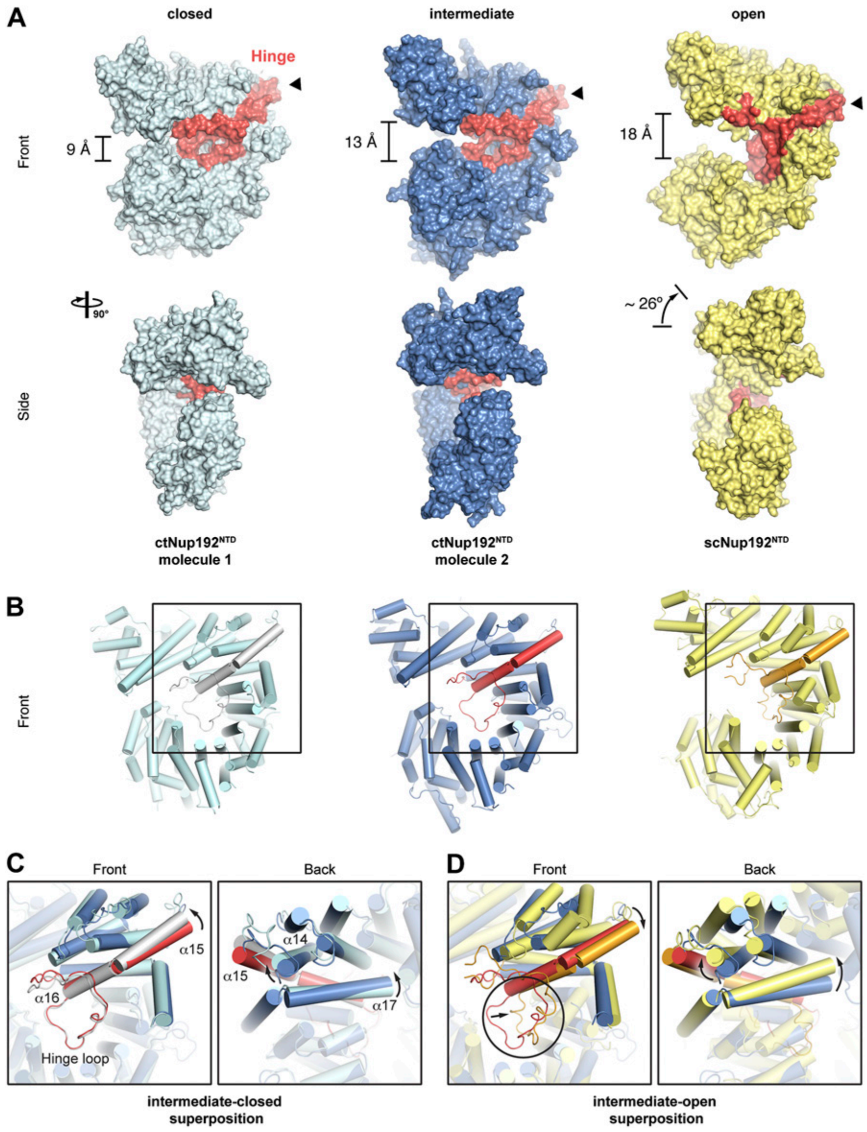

Fig. S4. Conformational plasticity of Nup192^{NTD}. (*A*) Structures of ctNup192^{NTD} (*Left* and *Center*) and scNup192^{NTD} (*Right*; PDB ID code 4IFQ) (1) are depicted in a surface representation. Their alignment on the C-terminal ARM module reveals conformational changes that are accompanied by an increased opening of the ring. (*Upper*) Hinge module of each structure is colored in red and indicated by a black triangle. (*Lower*) Rotated views (90°) show that the Head and HEAT modules also rotate along an axis out of the plane of the ring, reminiscent of the opening of a lock washer. (*B*) Cartoon representations of ctNup192^{NTD} and scNup192^{NTD} are shown in the same orientation, with the same coloring and order as in *A*. (*C*) Superposition of the closed and intermediate states of Nup192^{NTD}. (*D*) Superposition of the intermediate and open states of Nup192^{NTD}. (*Left*) Large change in the conformation of the hinge loop of scNup192^{NTD}, highlighted by the black circle, is propagated to the hinge helices (α15 and α16), causing the ring to adopt a further open state. Arrows indicate the observed conformational changes of the hinge helices from the closed state, to the intermediate state, to the open state.

1. Sampathkumar P, et al. (2013) Structure, dynamics, evolution, and function of a major scaffold component in the nuclear pore complex. *Structure* 21(4):560–571.

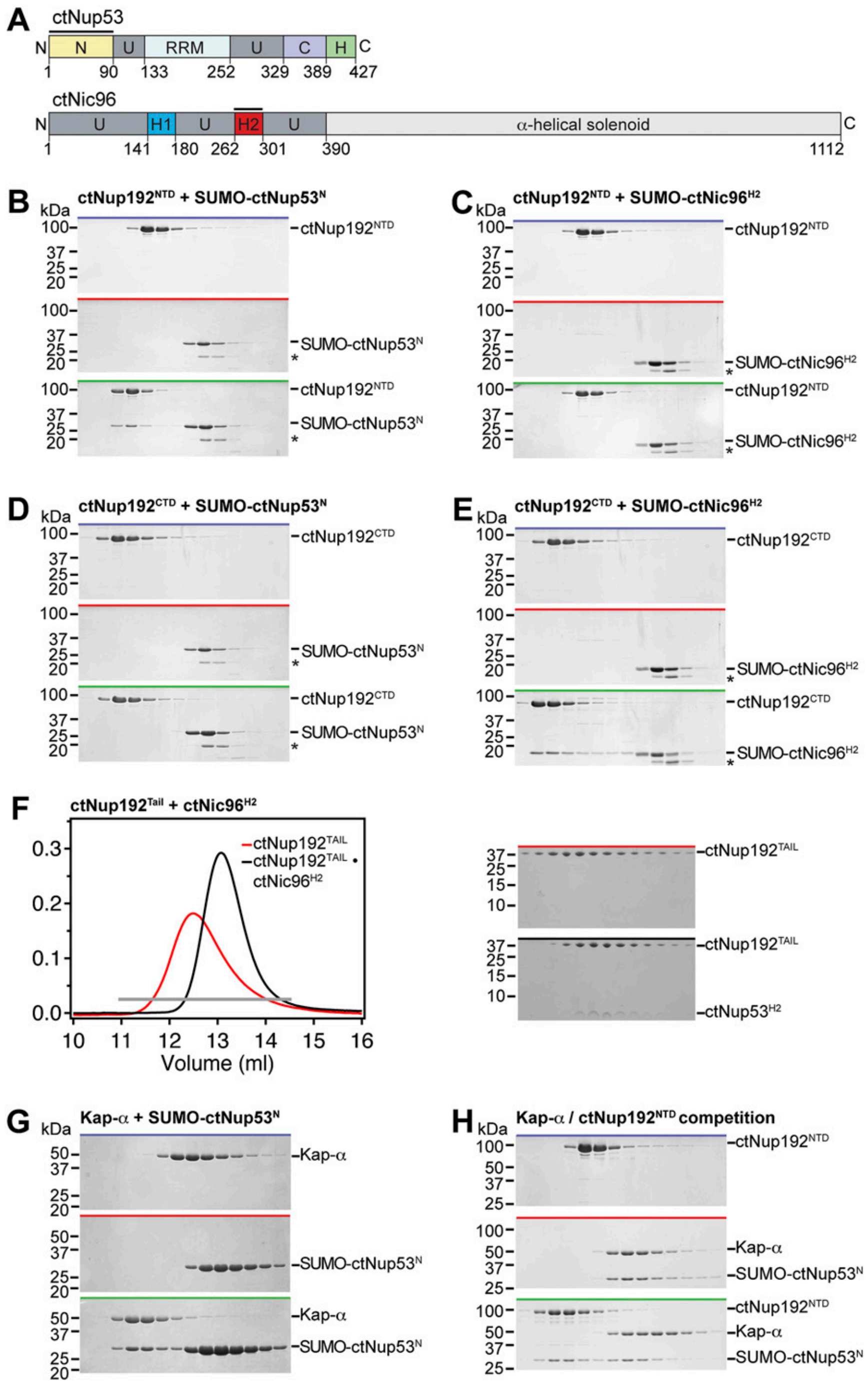

Fig. S5. Biochemical analysis of ctNup192 interactions. (*A*) Schematic overview of the domain organization of *C. thermophilum* Nup53 and Nic96. C, C-terminal segment; H, amphipathic helix; H1, Helix 1; H2, Helix 2; N, N-terminal segment; RRM, RNA-recognition motif domain; U, unstructured segment. (*B–E*) SDS/PAGE gels corresponding to the fractions indicated by gray bars in the gel filtration profiles of Fig. 4 *B–E*. (*F*) Interaction between ctNup192^{TAIL} and ctNic96^{H2}. SEC profiles of purified ctNup192^{TAIL} alone or the purified ctNup192^{TAIL}•ctNic96^{H2} complex are shown (*Left*), with the corresponding SDS/PAGE gels shown (*Right*). The gray bar indicates the fractions analyzed. (*G* and *H*) SDS/PAGE gels corresponding to the fractions indicated by gray bars in the gel filtration profiles of Fig. 4 *F* and *G*. Molecular mass standards and the positions of the proteins are indicated. Asterisks indicate degradation products of SUMO-ctNic96^{H2}. SDS/PAGE gels were stained with Coomassie brilliant blue.

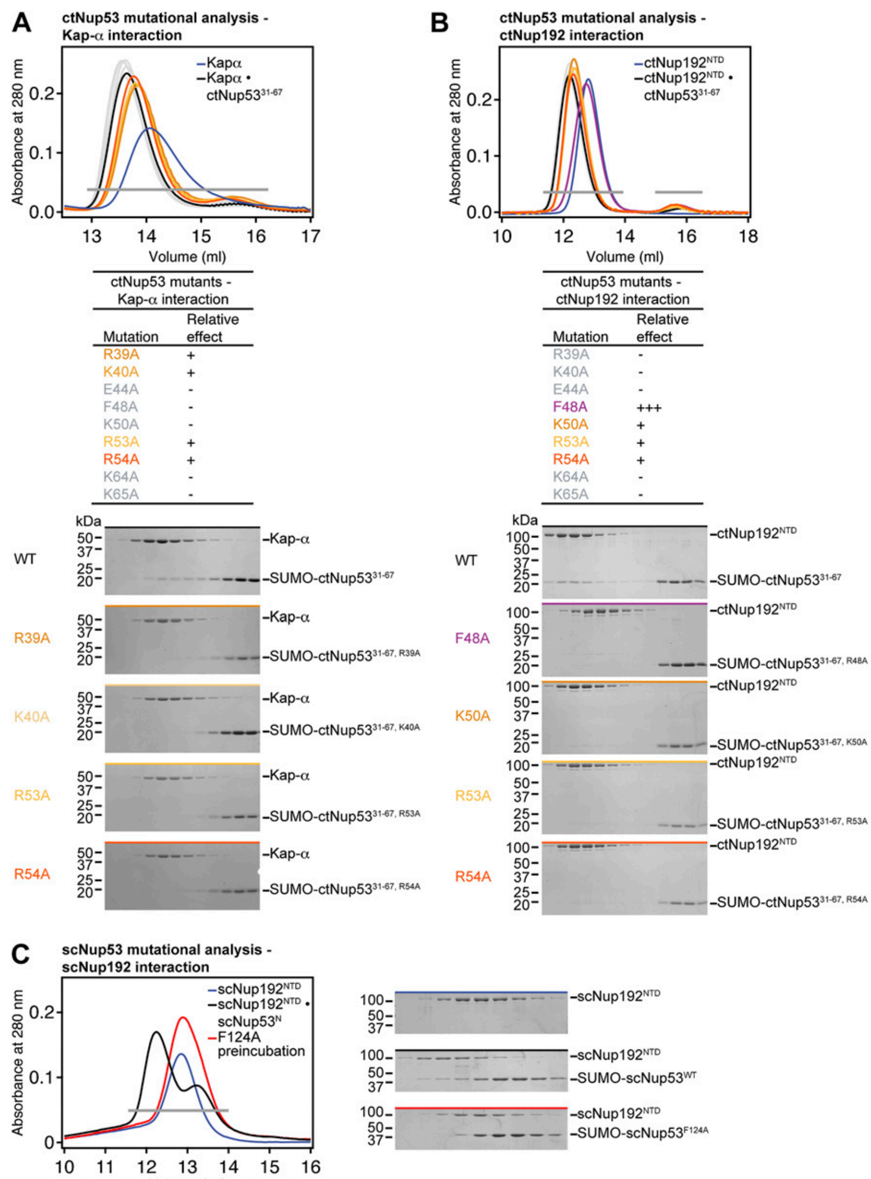

Fig. S6. Mutational analysis of Nup53 interactions. SEC interaction profiles of ctNup53$^{31–67}$ mutants and their effect on Kap-α (*A*) and ctNup192^{NTD} (*B*) binding. The results are summarized in Fig. 5*A*. Relative effects are categorized as no effect (–), reduced binding (+), and complete disruption (+++). Gray bars indicate fractions analyzed by Coomassie brilliant blue-stained gels. The corresponding gel filtration profiles are indicated by the colored bar above each gel. Molecular mass standards and the positions of the proteins are indicated. (*C*) Mutational analysis of *S. cerevisiae* Nup192^{NTD} and Nup53. The corresponding mutation F124A in scNup53^{N} also disrupts binding to scNup192^{NTD}, as shown by SEC analysis.

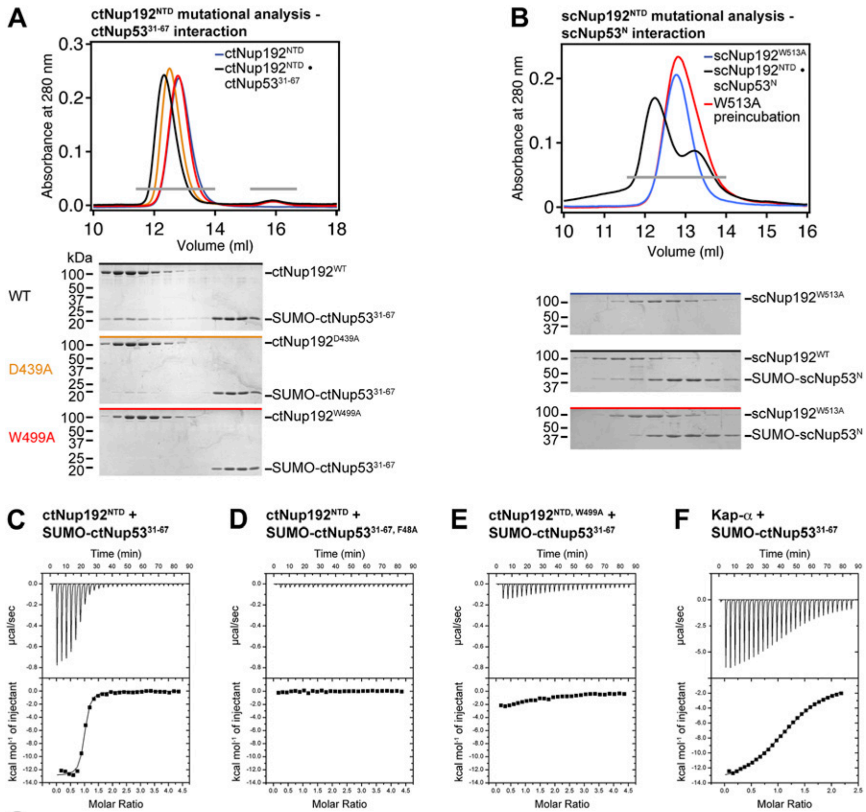

G

Isothermal titration calorimetry measurements				
Cell	ctNup192^{NTD}	ctNup192^{NTD}	ctNup192$^{NTD, W499A}$	Kap-α
Syringe	SUMO-ctNup53$^{31-67}$	SUMO-ctNup53$^{31-67, F48A}$	SUMO-ctNup53$^{31-67}$	SUMO-ctNup53$^{31-67}$
K_d (µM)	0.10 ± 0.02	ND[a]	ND[a]	25.3 ± 1.4
ΔH (kcal/mol)	-1.30 ± 0.16	-	-	-1.41 ± 0.15
ΔS (cal/mol/deg)	-12.0	-	-	-26.9
N (sites)	0.95 ± 0.01	-	-	1.34 ± 0.01

[a] ND, not determined

Fig. S7. Mutational analysis of Nup192^{NTD} interactions. (*A*) Representative SEC interaction profiles of ctNup192^{NTD} mutants and their effect on ctNup53$^{31–67}$ binding. Results are summarized in Fig. 5*B*. Representative gel filtration profiles illustrating reduced binding and complete disruption of the interaction are shown in orange and red, respectively. Gray bars indicate fractions analyzed by Coomassie brilliant blue-stained gels. The corresponding gel filtration profiles are indicated by the colored bar above each gel. Molecular mass standards and the positions of the proteins are indicated. (*B*) Mutational analysis of scNup192^{NTD} and Nup53. The corresponding mutation W513A in scNup192^{NTD} also disrupts binding to scNup53^{N}, as shown by SEC analysis. (*C*–*F*) ITC analysis of ctNup53$^{31–67}$ interactions. (*G*) Summary of the thermodynamic parameters determined using a single-site model.

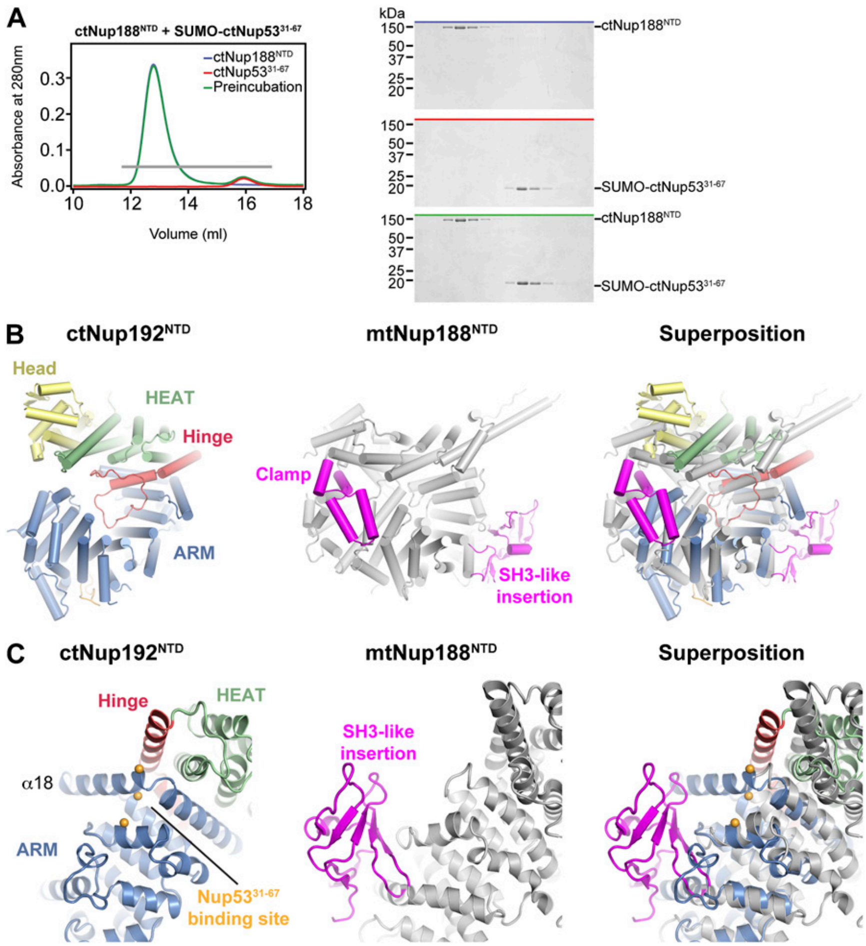

Fig. S8. Structural basis for distinct large adaptor nucleoporin binding specificity. (*A*) SEC analysis of the interaction between ctNup188^{NTD} and ctNup53$^{31–67}$. Gray bars and colored lines (*Left*) designate the analyzed fractions in the respective Coomassie brilliant blue-stained SDS/PAGE gels (*Right*). Molecular mass standards and the positions of the proteins are indicated. (*B*) Cartoon representations of ctNup192^{NTD} (*Left*), *Myceliophthora thermophila* Nup188^{NTD} (mtNup188^{NTD}, *Center*; PDB ID code 4KF7) (1), and their superposition (*Right*) are shown. The mtNup188^{NTD}-specific insertions are colored in magenta. (*C*) Comparison of the ctNup53 binding site in ctNup192^{NTD} with the corresponding location in mtNup188^{NTD}, colored as in *B*.

1. Andersen KR, et al. (2013) Scaffold nucleoporins Nup188 and Nup192 share structural and functional properties with nuclear transport receptors. *Elife* 2:e00745.

Table S1. Data collection and refinement statistics

	Native	Selenomethione peak	$[Ta_6Br_{12}]^{2+}$ peak
Data collection			
Protein	ctNup192^{NTD}	ctNup192^{NTD}	ctNup192^{NTD}
Synchrotron	SSRL*	SSRL	SSRL
Beamline	BL12-2	BL12-2	BL12-2
Space group	$P4_32_12$	$P4_32_12$	$P4_32_12$
Cell dimensions			
a, *b*, *c* (Å)	102.9, 102.9, 443.1	102.7, 102.7, 443.1	103.0, 103.0, 445.3
α, β, γ (°)	90.0, 90.0, 90.0	90.0, 90.0, 90.0	90.0, 90.0, 90.0
Wavelength	1.0000	0.9795	1.2547
Resolution (Å)	50.0 – 2.70	50.0 – 3.40	50.0 – 3.60
R_{sym} (%)†	9.5 (100.0)	12.7 (93.4)	11.9 (83.2)
$< I > / < \sigma I >$†	21.6 (3.1)	12.4 (2.0)	19.2 (4.0)
Completeness (%)†	100.0 (100.0)	99.9 (100.0)	100.0 (100.0)
No. of observations	859,560	235,738	474,247
No. of unique reflections†	66,696 (6,506)	33,944 (3,334)	28,901 (2,801)
Redundancy†	12.9 (12.9)	6.9 (7.0)	16.4 (16.0)
Refinement			
Resolution (Å)	50.0 – 2.70		
No. of reflections	66,555		
No. of reflections test set	3,390		
R_{work} / R_{free}	19.2 / 23.1		
No. atoms (non-hydrogen)	14,574		
Protein	14,202		
Water	297		
Ligand/Ions	75		
B-factors			
Protein	70.2		
Water	49.1		
RMSD			
Bond lengths (Å)	0.002		
Bond angles (°)	0.569		
Ramachandran plot‡			
Favored (%)	96.1		
Additionally allowed (%)	3.9		
Outliers (%)	0.0		

*SSRL, Stanford Synchrotron Radiation Lightsource.
†Highest-resolution shell is shown in parentheses.
‡As determined by MolProbity (1).

1. Davis IW, et al. (2007) MolProbity: All-atom contacts and structure validation for proteins and nucleic acids. *Nucleic Acids Res* 35(Web Server issue):W375–W383.

Table S2. Bacterial expression constructs

Protein	Residues (mutations if applicable)	Expression vector	Restriction sites 5′, 3′	N-terminal overhang
ctNup192^{NTD}	1–958	pET28a-PreS*	NdeI, NotI	GPH
ctNup192^{CTD}	976–1,756	pET28a-PreS	NdeI, NotI	GPHM
ctNup192^{TAIL}	1,358–1,756	pET28a-PreS	NdeI, NotI	GPHM
ctNup192$^{\Delta HEAD}$	153–958	pET28a-PreS	NdeI, NotI	GPHM
ctNup188^{NTD}	1–1,134	pET28a-PreS	AseI, BamHI	GPHN
scNup192^{NTD}	1–960	pET28a-PreS	NdeI, NotI	GPH
ctNup53^{N}	1–90	pET28a-SUMO	BamHI, NotI	S
ctNup53$^{31–67}$	31–67	pET28a-SUMO	BamHI, NotI	S
scNup53^{N}	1–181	pET28a-SUMO	BamHI, NotI	S
ctNic96^{H2}	814–960	pET28a-SUMO	BamHI, NotI	S
ctNic96^{H2}	814–960	pET-MCN-SUMO	BamHI, NotI	S
ctNup53$^{31–67,\ R39A}$	31–67 (R39A)	pET28a-SUMO	BamHI, NotI	S
ctNup53$^{31–67,\ K40A}$	31–67 (K40A)	pET28a-SUMO	BamHI, NotI	S
ctNup53$^{31–67,\ E44A}$	31–67 (E44A)	pET28a-SUMO	BamHI, NotI	S
ctNup53$^{31–67,\ F48A}$	31–67 (F48A)	pET28a-SUMO	BamHI, NotI	S
ctNup53$^{31–67,\ K50A}$	31–67 (K50A)	pET28a-SUMO	BamHI, NotI	S
ctNup53$^{31–67,\ R53A}$	31–67 (R53A)	pET28a-SUMO	BamHI, NotI	S
ctNup53$^{31–67,\ R54A}$	31–67 (R54A)	pET28a-SUMO	BamHI, NotI	S
ctNup53$^{31–67,\ K64A}$	31–67 (K64A)	pET28a-SUMO	BamHI, NotI	S
ctNup53$^{31–67,\ R65A}$	31–67 (R65A)	pET28a-SUMO	BamHI, NotI	S
scNup53$^{N,\ F124A}$	1–181 (F124A)	pET28a-SUMO	BamHI, NotI	S
ctNup192$^{NTD,\ E295A}$	1–958 (E295A)	pET28a-PreS	NdeI, NotI	GPH
ctNup192$^{NTD,\ E335A}$	1–958 (E335A)	pET28a-PreS	NdeI, NotI	GPH
ctNup192$^{NTD,\ E427A}$	1–958 (E427A)	pET28a-PreS	NdeI, NotI	GPH
ctNup192$^{NTD,\ D431A}$	1–958 (D431A)	pET28a-PreS	NdeI, NotI	GPH
ctNup192$^{NTD,\ S435A}$	1–958 (S435A)	pET28a-PreS	NdeI, NotI	GPH
ctNup192$^{NTD,\ N436A}$	1–958 (N436A)	pET28a-PreS	NdeI, NotI	GPH
ctNup192$^{NTD,\ D480A}$	1–958 (D480A)	pET28a-PreS	NdeI, NotI	GPH
ctNup192$^{NTD,\ E487A}$	1–958 (E487A)	pET28a-PreS	NdeI, NotI	GPH
ctNup192$^{NTD,\ D488A}$	1–958 (D488A)	pET28a-PreS	NdeI, NotI	GPH
ctNup192$^{NTD,\ N492A}$	1–958 (N492A)	pET28a-PreS	NdeI, NotI	GPH
ctNup192$^{NTD,\ D439A}$	1–958 (D439A)	pET28a-PreS	NdeI, NotI	GPH
ctNup192$^{NTD,\ L441A}$	1–958 (L441A)	pET28a-PreS	NdeI, NotI	GPH
ctNup192$^{NTD,\ K443A}$	1–958 (K443A)	pET28a-PreS	NdeI, NotI	GPH
ctNup192$^{NTD,\ R445A}$	1–958 (R445A)	pET28a-PreS	NdeI, NotI	GPH
ctNup192$^{NTD,\ R452A}$	1–958 (R452A)	pET28a-PreS	NdeI, NotI	GPH
ctNup192$^{NTD,\ Y475A}$	1–958 (Y475A)	pET28a-PreS	NdeI, NotI	GPH
ctNup192$^{NTD,\ W486A}$	1–958 (W486A)	pET28a-PreS	NdeI, NotI	GPH
ctNup192$^{NTD,\ L497A}$	1–958 (L497A)	pET28a-PreS	NdeI, NotI	GPH
ctNup192$^{NTD,\ W499A}$	1–958 (W499A)	pET28a-PreS	NdeI, NotI	GPH
ctNup192$^{NTD,\ R502A}$	1–958 (R502A)	pET28a-PreS	NdeI, NotI	GPH
ctNup192$^{NTD,\ R503A}$	1–958 (R503A)	pET28a-PreS	NdeI, NotI	GPH
ctNup192$^{NTD,\ F532A}$	1–958 (F532A)	pET28a-PreS	NdeI, NotI	GPH
ctNup192$^{NTD,\ F562A}$	1–958 (F562A)	pET28a-PreS	NdeI, NotI	GPH
ctNup192$^{NTD,\ E592A}$	1–958 (E592A)	pET28a-PreS	NdeI, NotI	GPH
ctNup192$^{NTD,\ M598A}$	1–958 (M598A)	pET28a-PreS	NdeI, NotI	GPH
ctNup192$^{NTD,\ Y602A}$	1–958 (Y602A)	pET28a-PreS	NdeI, NotI	GPH
ctNup192$^{NTD,\ E747A}$	1–958 (E747A)	pET28a-PreS	NdeI, NotI	GPH
ctNup192$^{NTD,\ R754A}$	1–958 (R754A)	pET28a-PreS	NdeI, NotI	GPH
ctNup192$^{NTD,\ L925A}$	1–958 (L925A)	pET28a-PreS	NdeI, NotI	GPH
ctNup192$^{NTD,\ L928A}$	1–958 (L928A)	pET28a-PreS	NdeI, NotI	GPH
ctNup192$^{NTD,\ V931A}$	1–958 (V931A)	pET28a-PreS	NdeI, NotI	GPH
ctNup192$^{NTD,\ V932A}$	1–958 (V932A)	pET28a-PreS	NdeI, NotI	GPH
ctNup192$^{NTD,\ L953A}$	1–958 (L953A)	pET28a-PreS	NdeI, NotI	GPH
scNup192$^{NTD,\ W513A}$	1–960 (W513A)	pET28a-PreS	NdeI, NotI	GPH
scKap-α	88–530	pProEX-HTb†	BamHI, XhoI	GAMGS

PreS, prescission.

*Crystallization construct.

†scKap-α expression construct was a gift from Elena Conti (Max Planck Institute of Biochemistry, Martinsried, Germany) (1).

1. Conti E, Uy M, Leighton L, Blobel G, Kuriyan J (1998) Crystallographic analysis of the recognition of a nuclear localization signal by the nuclear import factor karyopherin alpha. *Cell* 94(2):193–204.

Table S3. Yeast expression constructs

Protein	Residues (mutations if applicable)	Shuffle vector	Restriction sites 5′, 3′	Selection
scNup192^{FL}	1–1,683	pRS416-mCherry	NotI, SacII	Ura
scNup192^{FL}	1–1,683	pRS415-GFP	NotI, SacII	Leu
scNup192^{NTD}	1–954	pRS415-GFP	NotI, SacII	Leu
scNup192^{CTD}	955–1683	pRS415-GFP	NotI, SacII	Leu
scNup192$^{\Delta TAIL}$	1–1,316	pRS415-GFP	NotI, SacII	Leu
scNup192$^{\Delta TAIL,\ W513A}$	1–1,316 (W513A)	pRS415-GFP	NotI, SacII	Leu
scNup192$^{FL,\ W513A}$	1–1,683 (W513A)	pRS415-GFP	NotI, SacII	Leu
scNup53^{FL}	1–475	pRS416-mCherry	BamHI, NotI	Ura
scNup53^{FL}	1–475	pRS415-GFP	BamHI, NotI	Leu
scNup53$^{FL,\ F124A}$	1–475	pRS415-GFP	BamHI, NotI	Leu

Ura, uracil.